MATERIALS CHEMISTRY
FRONTIERS

RESEARCH ARTICLE

View Article Online
View Journal | View Issue

Cite this: *Mater. Chem. Front.*, 2023, **7**, 2251

A room-temperature moisture-stabilized metal-free energetic ferroelectric material for piezoelectric generation†

Jun Wang, Xiao-Xian Chen, Le Ye, Ya-Ping Gong, Yu Shang and Wei-Xiong Zhang *

Metal-free molecule-based ferroelectrics that are degradable and exhibit tunable structures, low production costs, and "soft" textures have prospects for sensing and piezoelectric generation applications, but the instances integrating multiple functionalities are very rare. Herein, we proved that an energetic material based on ternary perchlorate salt, (1-methyl-1,4-diazabicyclo-[2.2.2]octane-1,4-diium)$(NH_4)(ClO_4)_3$ (DAP-M4), is simultaneously a rare room-temperature ferroelectric crystal with a low hygroscopicity (a weight increase of less than 0.02% under 100% relative humility), an ultrawide band gap of 5.4 eV, "soft" mechanical properties (Young's modulus less than 23.68 GPa), and an exploitable piezoelectricity (d_{34} = 5.24 pC N^{-1}). Moreover, its potential piezoelectric generation application was demonstrated by an easily fabricated DAP-M4/TPU (thermoplastic polyurethane) composite film with an open-circuit voltage of 3.5 V and a short-circuit current of 0.5 μA. Being a novel energetic ferroelectric material with simultaneously excellent energetic and optical–electrical properties, DAP-M4 provides an attractive possibility for assembling highly integrated functional and self-destructive devices, and inspires the design of next-generation multi-functional materials based on diverse molecular components.

Received 24th January 2023,
Accepted 10th March 2023

DOI: 10.1039/d3qm00072a

rsc.li/frontiers-materials

Introduction

Molecule-based piezoelectric materials, differing from conventional inorganic piezoelectric crystals such as lead zirconate titanate (PZT), barium titanate ($BaTiO_3$), and zinc oxide (ZnO),[1–10] generally feature a piezoelectric effect benefiting from polar molecular components, which can undergo a special polarization conversion under proper stress. Taking advantage of their tunable structure, low production cost, "soft" texture, and degradability, molecule-based piezoelectric materials have attracted increasing attention in recent years.[1,11–13] For a given molecule-based piezoelectric, it is currently possible to predict its mechanical and piezoelectric properties using first-principles calculations of density functional theory (DFT) and density functional perturbation theory (DFPT), respectively.[14–27] Recently, these calculations have greatly improved the understanding of the origin of crystal mechanics and piezoelectricity for several piezoelectrics, such as (*R*-/*S*-(*N*-methylbenzylaminium))$PbBr_3$, (Hmdabco)$(NH_4)X_3$ (Hmdabco^{2+} = 1-methyl-1,4-diazabicyclo-[2.2.2]-octane-1,4-diium, X = Cl, Br, or I), and (benzyltrimethylammonium)$_2CoBr_4$.[19,20,25,26] Moreover, with the advantage of lower manufacturing costs when compared with conventional inorganic piezoelectric crystals, several molecule-based piezoelectric crystals have been assembled into piezoelectric generation devices for harvesting environmental vibrational energy to meet the requirements for self-energy supply in low-power devices.[11,12,22,23,26,28–38]

It was found that ferroelectrics, belonging to a class of piezoelectrics in which the direction of spontaneous polarization can be reversed by an applied electric field[13] and following a ferroelectric group–subgroup relationship during phase transitions,[39,40] generally have a higher piezoelectric effect than non-ferroelectric ones, and are thus more desired in seeking advanced piezoelectric materials.[40–43] Since the discovery of Rochelle salt, molecule-based ferroelectrics have been considered attractive and environmentally friendly functional piezoelectric materials, and the metal-free piezoelectric materials are believed to be even more flexible, tunable, biodegradable, and biocompatible, *e.g.*, (Hmdabco)$(NH_4)I_3$.[13,40] Among the numerous metal-free molecule-based ferroelectric crystals discovered in the past years,[3,6,13,36,44–48] certain perchlorate-based ones have potential energetic properties from their rapid decomposition capacities.[3,45,47] Such a type of material simultaneously exhibits excellent electric properties, for self-energy supply or

MOE Key Laboratory of Bioinorganic and Synthetic Chemistry, School of Chemistry, Sun Yat-Sen University, Guangzhou 510275, China.
E-mail: zhangwx6@mail.sysu.edu.cn

† Electronic supplementary information (ESI) available: Additional data and detail for piezoelectric generation test. CCDC 2234257, 2234258, and 2234259. For ESI and crystallographic data in CIF or other electronic format see DOI: https://doi.org/10.1039/d3qm00072a

information detection/processing, as well as good energetic properties, for self-destruction on demand, providing an attractive possibility to design highly integrated functional and self-destructive devices for the military. Nevertheless, the application of most of the known perchlorate-based ferroelectric crystals is limited due to their poor thermal stabilities or their high hygroscopicities under ambient conditions.[3,32,33,45]

We recently reported a family of metal-free perchlorate-based energetic materials possessing perovskite-type structures,[49] among which (Hmdabco)(NH_4)(ClO_4)$_3$ (called DAP-M4) has a good energetic performance and a rather high thermal stability (decomposition peak temperature T_d = 364 °C).[49] More interestingly, single-crystal structural analysis at 223 K preliminarily indicated that DAP-M4 crystallizes in a polar space group $P2_1$, implying potential ferroelectric properties. Herein, we comprehensively studied the structural phase transitions for DAP-M4, and proved that DAP-M4 is a rare room-temperature energetic ferroelectric, by means of thermal analyses, variable-temperature single-crystal X-ray diffraction, variable-temperature second-harmonic-generation (SHG), piezoresponse force microscopy (PFM), and first-principles calculations. Moreover, we found that the unique intermolecular interactions between the ternary molecular components endow DAP-M4 with a high moisture stability in air, differing from that of other known perchlorate-based ferroelectrics. Based on the piezoelectric characteristic of DAP-M4, we fabricated a DAP-M4/TPU (TPU = thermoplastic polyurethane) composite film to demonstrate its piezoelectric generation for harvesting environmental vibrational energy.

Experimental

Syntheses

DAP-M4, (Ac)ClO_4 (acetamidinium perchlorate), (Im)ClO_4 (imidazolium perchlorate), and (Hdabco)ClO_4 (1,4-diazabicyclo[2.2.2]octan-1-ium perchlorate) were synthesized according to methods reported in the literature.[3,45,49,50] The product purity was verified by powder X-ray diffraction (PXRD) patterns (Fig. S1 and S6, ESI†).

Materials and instruments

All chemicals were commercially available and used without further purification. PXRD patterns were recorded using a Bruker D8 ADVANCE X-ray powder diffractometer (Cu Kα, λ = 1.54184 Å). DSC measurements were performed by heating/cooling the powder samples at a rate of 10 K min^{-1} on a TA DSC Q2000 instrument. The second-harmonic-generation (SHG) effect was measured using a XPL1064-200 instrument at a heating/cooling rate of 5 K min^{-1}. The temperature-dependent dielectric permittivity was performed for a tablet powder sample on a Tonghui TH2828A instrument at a frequency range from 50 to 1000 kHz with an applied electric field at 1 V. Ferroelectric hysteresis loops were measured on a Radiant Precision Premier II instrument. PFM measurements were performed by using a PFM mode on a Bruker Dimension Fast Scan Bio Atomic Force Microscope. The cross-sectional photographs and compositional analysis of the flexible films were characterized by Zeiss Gemini 500 and Flat-QUAD EDS, respectively. The UV-vis spectrum was measured on a Perkin-Elmer (British) Lambda 950 spectrophotometer at room temperature. The band gap (E_g) was estimated by converting reflectance data into absorbance with the Kubelka–Munk equation: $(h\nu \cdot F(R_\infty))^{1/n} = A(h\nu - E_g)$.

Single-crystal X-ray diffraction analyses

Diffraction data were collected on a SuperNova single-crystal diffractometer by using Cu Kα (λ = 1.54184 Å) radiation. Absorption corrections were applied by using the multi-scan program CrysAlisPro. All structures were solved by the direct methods and refined by the full-matrix least-squares technique with the SHELX program package on Olex.[2] Anisotropic thermal parameters were applied to all non-hydrogen atoms. The hydrogen atoms were generated geometrically. Crystal data and refinements for DAP-M4 are summarized in Table S1 (ESI†).

Hygroscopicity measurements

The hygroscopicity was determined by the weight gain method.[51] About 2 g of ground test samples were initially dried to a constant weight (with a fluctuation less than 0.2 mg) and then placed in chambers at room temperature and a relative humidity of 43%, 67%, 86%, and 100%, respectively. The samples were weighed every 12 h. The moisture absorption rate ω was calculated by the following equation.

$$\omega = \frac{m_1 - m_0}{m_0} \times 100\%$$

where m_0 denotes the initial mass, g; and m_1 denotes the mass after moisture absorption, g.

Piezoelectric generation

A powder sample (1.0 g) of DAP-M4 was added to a tetrahydrofuran solution (1 mL) containing 21.9 wt% TPU and stirred for 2 h. Then, the mixture was placed in a vacuum oven to drain the bubbles generated by stirring, before spreading it on the glass substrate. Finally, the 250 μm-thick DAP-M4/TPU composite flexible film was obtained. A piezoelectric generator consisting of the DAP-M4/TPU composite film with both top and bottom copper tapes attached by conductive wires was fabricated. The piezoelectric generations were demonstrated by a magnetic shaker, and the generator device was operated by a periodic external force of 30 N from the shaker (shown in Fig. S14a, ESI†). The conductive wires from both of the electrodes were fixed through a cable and directly connected to a megger (Keithley 6517B) to collect the output voltage and current signal during the measurement.

Computational details

The elastic and piezoelectric constants were obtained by first-principles calculations based on density functional theory (DFT), which were performed using the Vienna *ab initio* simulation package (VASP). The energy cut-off was set to 500 eV, and the *k*-point mesh spanning scheme of Monkhorst–Pack was 3 × 3 × 2. Local density approximation was used as the

exchange–correlation energy functional to optimize the atomic positions in different pressure conditions when the lattice parameters were fixed to the experimental values. The elastic stiffness constants were obtained by the finite-strain method with 0.015 Å of the maximum strain amplitude and six steps for each strain. The maximum force and the total energy converged to 0.02 eV $Å^{-1}$ and 10^{-6} eV for a single atom, respectively. The zero-damping DFT-D3 method combined with the Grimme correlation was applied to explicate the discrete effects. The piezoelectric strain constants (d_{ij}) were obtained by the formula $d_{ij} = e_{ij} \times s_{ij}$, where e_{ij} (the piezoelectric stress tensor) was calculated using density functional perturbation theory (DFPT), and s_{ij} is the elastic compliance constant (the inverse matrix of the elastic stiffness constant). The band structure and partial density of states (PDOS) of DAP-M4 were obtained by DFT calculations, and the piezopotential was simulated by COMSOL.

Results and discussion

Two reversible structural phase transitions were detected by DSC curves during a heating/cooling cycle (Fig. 1), as indicated by two pairs of thermal anomalies at around 356/355 K and 361/358 K, respectively. The total entropy changes (ΔS) during the two-step phase transitions in the heating run were estimated to be 1.1 and 10.5 J mol^{-1} K^{-1}, respectively. For convenience, we labeled the phase at below 356 K, between 356 K and 361 K, and above 361 K as RTP, ITP, and HTP, respectively.

To visually understand these structural phase transitions, variable-temperature single-crystal X-ray diffractions were performed at 293, 358, and 393 K for RTP, ITP, and HTP, respectively (Fig. 2). Crystal data as well as details of data collection and refinements for DAP-M4 are summarized in Table S1 (ESI†). In general, DAP-M4 adopts an ABX_3-type perovskite structure, in which each B-site cation (NH_4^+) is surrounded by six X-site anions (ClO_4^-) to form a three-dimensional inorganic framework consisting of cages occupied by A-site organic cations ($Hmdabco^{2+}$). The structure collected at 293 K (RTP) crystallizes in space group $P2_1$ with a = 10.20664 Å, b = 11.00567 Å, c = 14.84750 Å, and β = 90.1263°, which is consistent with the our previously reported structure at 223 K, except that the cell at 293 K is slightly expanded.[49] In the RTP, the $(NH_4)(ClO_4)_6$ octahedra are slightly distorted, and the A-site organic cations are crystallographically ordered.

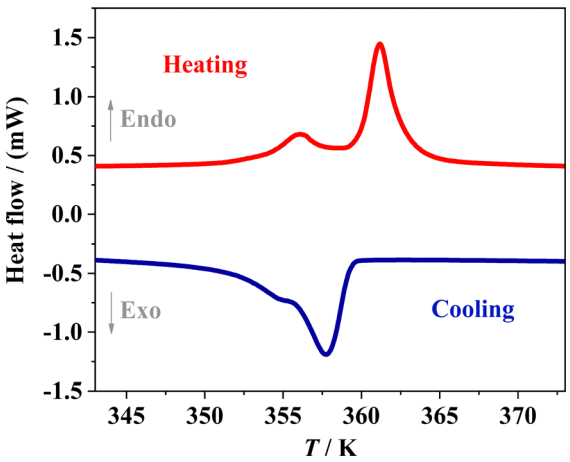

Fig. 1 DSC curves for DAP-M4 during a heating/cooling cycle.

The two-step structural phase transitions were found to be highly associated with the gradually activated molecular dynamics of A-site $Hmdabco^{2+}$ cations with increasing temperature. In detail, the structure collected at 358 K (ITP) belongs to the trigonal space group $R\bar{3}m$ with a = 10.6675 Å and c = 13.0585 Å, in which the organic cations are 12-fold dynamically disordered in almost arbitrary orientations and the $(NH_4)(ClO_4)_6$ octahedra become regular.[52] With further heating, the HTP belongs to the cubic space group $Pm\bar{3}m$ with a = 7.5679 Å, which is a prototype of a typical perovskite structure without any deformation, and, accordingly, the $Hmdabco^{2+}$ cations, NH_4^+ cations, and ClO_4^- bridges are 48-fold, 48-fold, and 16-fold dynamically disordered, respectively. Such stepwise changes in the molecular dynamic motions agree with the aforementioned entropy changes during phase transitions observed in DSC curves. It is worth noting that the phase transition from ITP to RTP belongs to an Aizu notation of $\bar{3}mF2$, which is a ferroelectric transition with a number change of symmetry elements from 12 (E, $2C_3$, $3C_2'$, i, 2S6, and $3\sigma_d$) to 2 (E and C_2), suggesting DAP-M4 is an uncommon multi-axial ferroelectric with three ferroelectric axes in RTP.[53]

To further clarify the ferroelectric properties of RTP, a variable-temperature SHG measurement was performed on the polycrystalline sample of DAP-M4 (shown in Fig. 3a). The SHG intensity at 298 K (RTP) is about 0.23 times that of the reference KH_2PO_4. When heated to above 356 K (ITP), the SHG intensity decreases to almost zero, *i.e.*, the SHG is silenced. Such a SHG switch behavior fits well with the space group variation between the non-centrosymmetric RTP ($P2_1$) and the centrosymmetric ITP ($R\bar{3}m$) observed in single-crystal X-ray diffraction. In addition, the temperature dependence of the real part of the dielectric permittivity (ε') was evaluated in the range of 295–392 K on a powder-pressed sample of DAP-M4 (as shown in Fig. 3b). It exhibits a reversible step-like dielectric response between RTP and HTP in a heating–cooling cycle, which is an indication of an improper ferroelectric.[41,52]

Moreover, the variable-temperature electric polarization *versus* electric field (P–E) hysteresis loops (Fig. S2, ESI†) were measured on a single crystal by applying an electric field along its b axis (*i.e.*, the polarization axis), revealing that the polarization value at an electric field of 5 kV cm^{-1} was significantly decreased from 2.31 μC cm^{-2} at 293 K (ferroelectric RTP) to 0.52 μC cm^{-2} at 358 K (paraelectric ITP). It should be noted that the spontaneous polarization measured at 293 K was not saturated yet under an electric field of 5 kV cm^{-1}, owing to the relatively larger electric field required for overcoming the spatial resistance to rotate the $Hmdabco^{2+}$ cations.

To gain insight into the ferroelectric domain distribution in RTP, both vertical and lateral PFM (VPFM and LPFM) mappings[54] were investigated on the same region (5 μm × 5 μm) of the DAP-M4

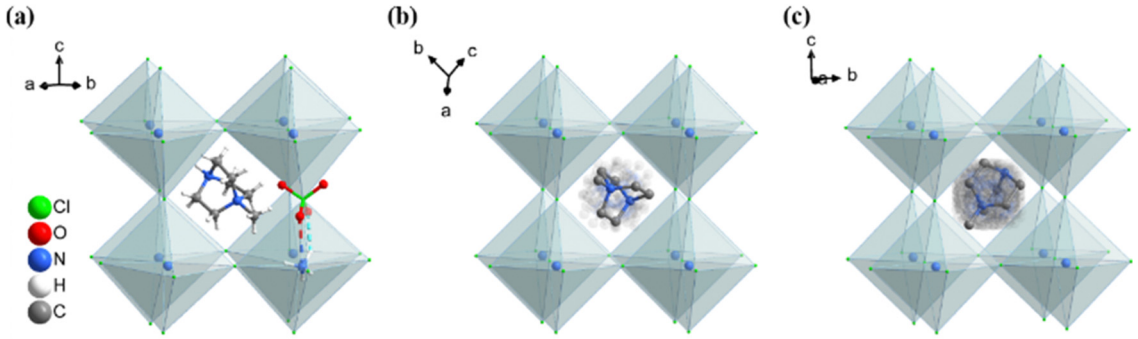

Fig. 2 Crystal structure of DAP-M4 at (a) RTP, (b) ITP, and (c) HTP. Hydrogen atoms are omitted for clarity.

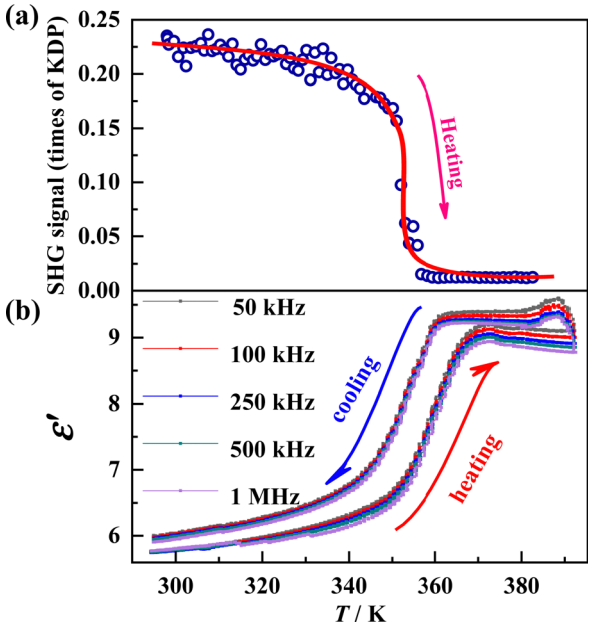

Fig. 3 (a) Temperature-dependence of the SHG signal in a heating run and (b) real part of the dielectric permittivity during a cooling–heating cycle measured under an ac electric field for DAP-M4.

single crystal by applying a voltage perpendicular to the crystal plane (shown in Fig. S3, ESI†). Obviously, a bipolar domain pattern emerged in the VPFM amplitude and phase, indicating the presence of two different 180° polarization directions in the region.[8,52] Similarly, the LPFM amplitude image shows a bipolar domain distribution while the LPFM phase signal is blurred and distorted. The distinctive domain distributions of the VPFM and LPFM mappings suggested that DAP-M4 is an anti-parallel polarized ferroelectric along the polar axis. Therewith, to manifest the polarization reversal behavior, the ultrafast reversal trend of DAP-M4 ferroelectric polarization clearly emerges (Fig. 4). The tip bias was separately applied at −1 V, 0 V, and +1 V, respectively, in three equal regions, which results in two significant reversals in the polarization direction visible in the VPFM and LPFM phases (shown in Fig. 4c, f and Fig. S4, ESI†). Moreover, when the applied voltage was 8 V (*E* is *ca.* 57 kV cm^{-1}), a slender phase loop and an amplitude loop (Fig. 4d) representing the ultrafast polarization reversal of domains were observed. In short, these observations confirmed the fast reversal of ferroelectric polarization for DAP-M4, distinguishing it from other piezoelectric/pyroelectric materials. To the best of our knowledge, DAP-M4 is the first energetic ferroelectric based on ternary perchlorate salt.

The hygroscopicity of DAP-M4 was further investigated at ambient temperature and under 43%, 67%, 86%, 100% relative humidity (RH), respectively. For comparison, three known potential energetic ferroelectric and polar materials based on binary perchlorate salts, *i.e.*, (Ac)ClO_4 (acetamidinium perchlorate),[50] (Im)ClO_4 (imidazolium perchlorate),[45,47] and (Hdabco)ClO_4 (1,4-diazabicyclo-[2.2.2]octan-1-ium perchlorate),[3] were also investigated under the same conditions. The results (Fig. S5, ESI†) indicated well that DAP-M4 has a much higher moisture stability than the other three compounds. For instance, when staying at 67% RH for 144 hours, (Ac)ClO_4, (Im)ClO_4, and (Hdabco)ClO_4 increased by 1.97%, 0.26% and 0.044% in weight, respectively, while DAP-M4 increased by only 0.01%,with error bars of about 0.02%. Even under 100% RH for after 144 hours, as shown in Fig. 5, DAP-M4 only achieved a 0.01% weight increase, which is far below that of (Ac)ClO_4 (2.96%), (Im)ClO_4 (0.87%), and (Hdabco)ClO_4 (0.3%). In short, compared with these binary perchlorate ferroelectric compounds, DAP-M4, as a ternary perchlorate salt, has a good non-humidity dependence and maintains ultra-low hygroscopicity even at 100% RH, and is preferable to its un-methylated prototype compound (*i.e.*, (H_2dabco)(NH_4)(ClO_4)$_3$ called DAP-4) with a weight gain of 0.06% at 90% RH.[51,55]

To determine the mechanism for the moisture stability of DAP-M4, Hirshfeld surface analysis was performed for the organic Hmdabco^{2+} cation in RTP (shown in Fig. S7, ESI†). The H atoms from both the Hmdabco^{2+} cation and the NH_4^+ cation interact with the O atoms from ClO_4^- *via* N/C–H···O hydrogen bonds, such that the cations and anions alternately complement each other and closely pack in a dense crystal structure. Such complementing inner hydrogen bonds, together with the hydrophobic methyl groups, prevent the H and O atoms in NH_4^+ and ClO_4^- from forming strong hydrogen bonds with water molecules in the air, thus endow DAP-M4 with ultra-low hygroscopicity.[49,55,56]

The UV–vis absorption spectrum was measured on the polycrystalline sample (Fig. S8a, ESI†), and the partial density of states (PDOS) and the band structure were calculated

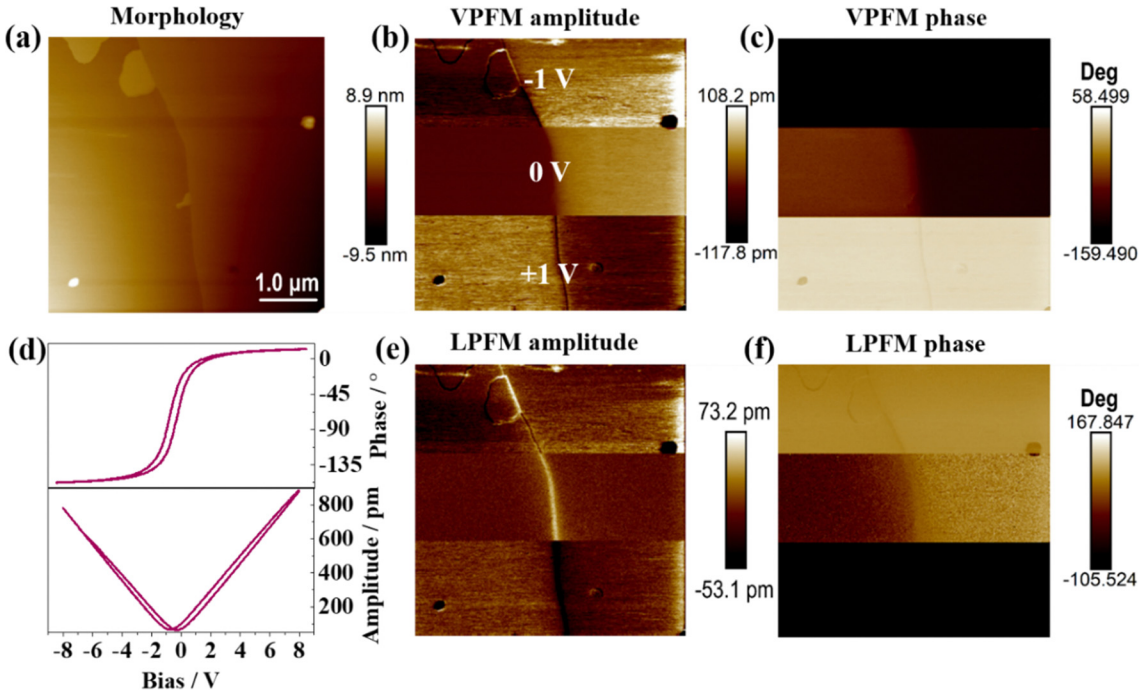

Fig. 4 (a) Morphology image, and (b and c) vertical and (e and f) lateral PFM images of the crystal surface for DAP-M4. (d) Phase–voltage hysteresis loop and amplitude–voltage loop for a selected area on the crystal surface.

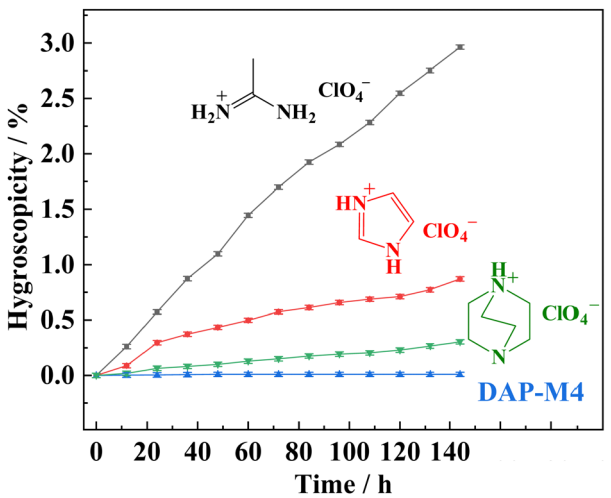

Fig. 5 Hygroscopic curves of $(Ac)ClO_4$, $(Im)ClO_4$, $(Hdabco)(ClO_4)$, and DAP-M4 at room temperature under 100% RH.

(Fig. S8b and c, ESI†) based on the single-crystal structure to estimate the band gap for DAP-M4. The UV-vis absorption spectrum indicated progressively absorbing edges at about 230 nm, and a band gap of 5.40 eV was estimated (the inset plot in Fig. S8a, ESI†). The conduction-band minimum (CBM) and the valence-band maximum (VBM) lie in different positions in the Brillouin zone, indicating that DAP-M4 is an indirect band gap semiconducting material, and the band gap calculated from the difference between CBM and VBM is 5.40 eV, which is in good agreement with the value obtained by the UV-vis absorption spectrum. As revealed by the PDOS, the H-1s states overlap fully with C-2s2p and N-2s2p in the energy ranges of −21 to 16.5 eV, indicating strong covalent interactions of the C–H and N–H. The CBM and VBM are mainly from the O-2p states and the Cl-3p states, respectively. Namely, the band gap of DAP-M4 is mainly determined by the ClO_4^- anions. These facts indicated that DAP-M4 has an ultrawide band gap, exceeding GaN (3.4 eV) and $(benzylammonium)_2PbCl_4$ (3.65 eV), but slightly lower than diamond (5.47 eV), and offers potential applications in extreme environments.[57–60]

As an energetic ferroelectric material, DAP-4 may serve as a promising molecule-based piezoelectric material with excellent electro-mechanical coupling properties. For a piezoelectric material, the elastic properties are of particular importance as they reflect not only the resistance to stresses in various directions, but also facilitate further characterization of the intrinsic piezoelectric properties of the crystal. Nevertheless, little was known about the elastic properties of the promising metal-free piezoelectric materials.[25] In order to understand the elastic properties of DAP-M4, its elastic stiffness constants C_{ij} (in GPa) were calculated by DFT and are matrixed as follows:

$$\begin{pmatrix} 24.783 & 8.6 & 9.27 & 0 & -0.476 & 0 \\ 8.6 & 25.92 & 12.685 & 0 & -0.18 & 0 \\ 9.27 & 12.685 & 27.441 & 0 & 1.129 & 0 \\ 0 & 0 & 0 & 9.197 & 0 & -1.033 \\ -0.476 & -0.18 & 1.129 & 0 & 8.191 & 0 \\ 0 & 0 & 0 & -1.033 & 0 & 6.981 \end{pmatrix}$$

Based on the above C_{ij} values, the elastic properties, including Young's modulus (E), shear modulus (G), and Poisson's ratio (ν), are graphically depicted by the visualization

algorithm, as shown in Fig. S9 (ESI†), and the relevant extreme values are listed in Table S2 (ESI†). Young's modulus (E) characterizes the resistance of the crystal elastic deformation, and its maximum value (E_{max}) and minimum value (E_{min}) are 23.68 GPa and 17.08 GPa, respectively. For example, as shown in Fig. S10 (ESI†), along the ⟨−1−10⟩ direction, the Cl atoms in the ClO_4^- anions are constituted at different angles to the N atom in the adjacent NH_4^+ ions, exhibiting spatial geometric asymmetry, and the distorted $(NH_4)(ClO_4)_6$ octahedra bring about different Young's moduli of the DAP-M4 crystal along different directions, *i.e.*, an anisotropic mechanical response. Likewise, for the shear modulus, representing the resistance of the material to shear deformation, the maximum value (G_{max}) is 9.60 GPa and the minimum value (G_{min}) is 6.57 GPa. Such a relatively minor difference between the maximum and minimum shear modulus could be mainly ascribed to the dense cubic crystal structure in DAP-M4. Namely, DAP-M4 has an advantage over metal-free $(Hmdabco)(NH_4)I_3$ (E_{max} = 19 GPa, E_{min} = 6.39 GPa) and discrete $(benzyltrimethylammonium)_2CoBr_4$ (E_{max} = 17.6 GPa, E_{min} = 4.11 GPa),[25,26] but also exhibits softer mechanical properties than $(Hmdabco)KI_3$ (E_{max} = 28.2 GPa, E_{min} = 22.5 GPa).[25]

With its "soft" mechanical properties, when DAP-M4 is subjected to an external stress, it tends to generate a large deformation and then a large piezoelectricity. The piezoelectric strain coefficients matrix obtained from the DFPT calculations demonstrated that the ion contribution is greater than the electric contribution to the piezoelectric stress tensor e_{ij} (Table S3, ESI†). Precisely, the motions of positive and negative ions under an applied electric field are mainly responsible for the potential shift. The 3D and 2D representations of the piezoelectric strain constants d_{ij} are shown in Fig. 6a and b, and the specific values of d_{ij} (unit of pC N^{-1}) matrix are as follows.

$$\begin{pmatrix} 0 & 0 & 0 & -0.71 & 0 & -0.1 \\ -0.42 & -0.86 & -0.12 & 0 & 0.01 & 0 \\ 0 & 0 & 0 & 5.24 & 0 & 0.77 \end{pmatrix}$$

In the d_{ij} matrix, the shearing piezoelectric constant d_{34} is 5.24 pC N^{-1}, which is 6 times larger than d_{14} of quartz.[26] The origin of piezoelectricity can be rationalized by the polar structure of RTP. In detail, since non-polar NH_4^+ and ClO_4^- of RTP are perfectly symmetrically aligned along the *a*, *b*, and *c* axes, the centers of positive and negative charges remain aligned when stress is applied, whereas the methyl group and the non-centrosymmetric arrangement of $Hmdabco^{2+}$ cations allow the perturbation of the external strain to easily split the centers of the positive and negative charges, producing a net dipole moment along the *b*-axis direction and generating a noticeable d_{34}.[16,20,21] The shear piezoelectric effects enable DAP-M4 to be a promising piezoelectric crystal to be assembled cooperatively with other materials for mechanical/electronic transformation in a power generation device.[61]

To demonstrate the potential piezoelectric generation applications for DAP-M4, a DAP-M4/TPU composite film (shown in Fig. S11, ESI†) was fabricated by integrating DAP-M4 crystal particles into thermoplastic polyurethane (TPU), which has good elasticity and toughness to serve as a gelling agent.[62] As shown in Fig. S12 and S13 (ESI†), comparative XRD patterns and the cross-sectional morphology of the DAP-M4/TPU composite films indicated that the TPU acts as an adhesive to bind DAP-M4 particles. In addition, an open-circuit voltage (V_{oc}) of about 3.5 V and a short-circuit current (I_{sc}) of about 0.5 μA were obtained by tapping the device with a sandwich structure consisting of a composite film layer and two copper foils within 600 s (as shown in Fig. S14, ESI†). For reference, the neat TPU polymer has a V_{oc} of 200 mV and a negligible I_{sc} value.[63] Moreover, the simulated piezoelectric potential maximum is relatively close to V_{oc} (as shown in Fig. S14c, ESI†). To more clearly represent the signal trends of V_{oc} and I_{sc}, the relatively stable piezoelectric generation of the DAP-M4/TPU film in 5 s (from 130 s to 135 s) is shown in Fig. 6c. Comparatively, the sensitivity performance of the DAP-M4/TPU film for piezoelectric generation (105 mV kPa^{-1}) is superior to a composite based on imidazolium perchlorate embedded in a bacterial cellulose hydrogel (4.24 mV kPa^{-1}).[32]

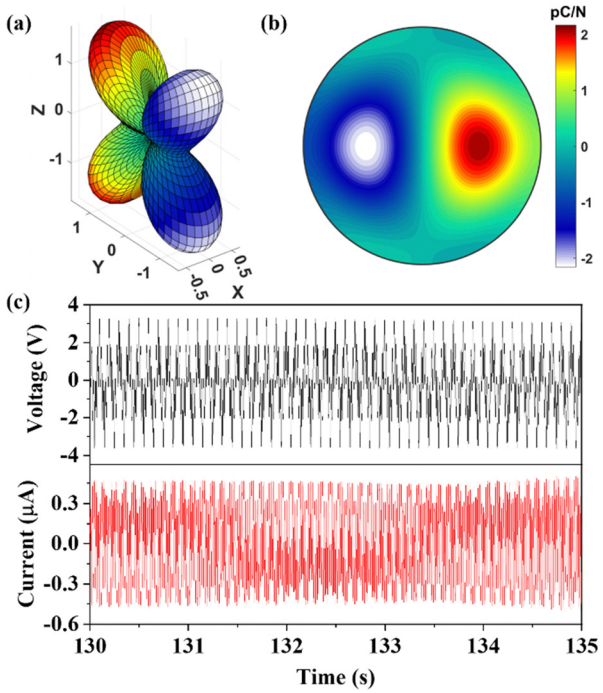

Fig. 6 (a) 3D and (b) 2D surface rendering representations of the piezoelectric strain tensors for DAP-M4. (c) Output of the open-circuit voltage (V_{oc}) and short-circuit current (I_{sc}) of DAP-M4/TPU film from 130 s to 135 s.

Conclusions

In summary, we proved that the energetic material DAP-M4 is a rare room-temperature moisture-stabilized ferroelectric crystal simultaneously exhibiting a low hygroscopicity, an ultrawide band gap, "soft" mechanical properties, and an exploitable piezoelectricity. By taking advantage of these properties, we

fabricated a DAP-M4/TPU composite film, which exhibits a V_{oc} of about 3.5 V and a I_{sc} of about 0.5 μA, thus demonstrating the potential of DAP-M4 to be used for self-energy supply or information detection/processing. The results suggest that DAP-M4, as a scarce instance of an energetic ferroelectric material simultaneously exhibiting excellent energetic and optic–electric properties, provides an attractive possibility for integrated functional and self-destructive devices in high-tech military equipment. The present studies on such types of novel energetic ferroelectric materials may inspire the design of next-generation integrated functional materials based on diverse molecular/ionic components.

Conflicts of interest

There are no conflicts to declare.

Acknowledgements

This work was supported by the NSFC (22071273 and 21821003), and the Local Innovative and Research Teams Project of Guangdong Pearl River Talents Program (2017BT01C161).

Notes and references

1 C. Shi, J. J. Ma, J. Y. Jiang, M. M. Hua, Q. Xu, H. Yu, Y. Zhang and H. Y. Ye, Large piezoelectric response in hybrid rare-earth double perovskite relaxor ferroelectrics, *J. Am. Chem. Soc.*, 2020, **142**, 9634–9641.

2 Y. Y. Tang, Y. Xie, Y. Ai, W. Q. Liao, P. F. Li, T. Nakamura and R. G. Xiong, Organic ferroelectric vortex-antivortex domain structure, *J. Am. Chem. Soc.*, 2020, **142**, 21932–21937.

3 Y. Y. Tang, W. Y. Zhang, P. F. Li, H. Y. Ye, Y. M. You and R. G. Xiong, Ultrafast polarization switching in a biaxial molecular ferroelectric thin film: [Hdabco]ClO_4, *J. Am. Chem. Soc.*, 2016, **138**, 15784–15789.

4 S. Wang, L. Li, W. Weng, C. Ji, X. Liu, Z. Sun, W. Lin, M. Hong and J. Luo, Trilayered lead chloride perovskite ferroelectric affording self-powered visible-blind ultraviolet photodetection with large zero-bias photocurrent, *J. Am. Chem. Soc.*, 2020, **142**, 55–59.

5 Z. X. Wang, H. Zhang, F. Wang, H. Cheng, W. H. He, Y. H. Liu, X. Q. Huang and P. F. Li, Superior transverse piezoelectricity in a halide perovskite molecular ferroelectric thin film, *J. Am. Chem. Soc.*, 2020, **142**, 12857–12864.

6 Z. H. Wei, Z. T. Jiang, X. X. Zhang, M. L. Li, Y. Y. Tang, X. G. Chen, H. Cai and R. G. Xiong, Rational design of ceramic-like molecular ferroelectric by quasi-spherical theory, *J. Am. Chem. Soc.*, 2020, **142**, 1995–2000.

7 Y. Xie, Y. Ai, Y. L. Zeng, W. H. He, X. Q. Huang, D. W. Fu, J. X. Gao, X. G. Chen and Y. Y. Tang, The soft molecular polycrystalline ferroelectric realized by the fluorination effect, *J. Am. Chem. Soc.*, 2020, **142**, 12486–12492.

8 W.-J. Xu, P.-F. Li, Y.-Y. Tang, W.-X. Zhang, R.-G. Xiong and X.-M. Chen, A molecular perovskite with switchable coordination bonds for high-temperature multiaxial ferroelectrics, *J. Am. Chem. Soc.*, 2017, **139**, 6369–6375.

9 Y. Zhang, W. Zhang, S. H. Li, Q. Ye, H. L. Cai, F. Deng, R. G. Xiong and S. D. Huang, Ferroelectricity induced by ordering of twisting motion in a molecular rotor, *J. Am. Chem. Soc.*, 2012, **134**, 11044–11049.

10 Z. L. Wang and J. Song, Piezoelectric nanogenerators based on zinc oxide nanowire arrays, *Science*, 2006, **312**, 242–246.

11 B. Wang, J. Hong, Y. Yang, H. Zhao, L. Long and L. Zheng, Achievement of a giant piezoelectric coefficient and piezoelectric voltage coefficient through plastic molecular-based ferroelectric materials, *Matter*, 2022, **5**, 1296–1304.

12 Y. Zhang, X.-J. Song, Z.-X. Zhang, D.-W. Fu and R.-G. Xiong, Piezoelectric energy harvesting based on multiaxial ferroelectrics by precise molecular design, *Matter*, 2020, **2**, 697–710.

13 H. Y. Ye, Y. Y. Tang, P. F. Li, W. Q. Liao, J. X. Gao, X. N. Hua, H. Cai, P. P. Shi, Y. M. You and R. G. Xiong, Metal-free three-dimensional perovskite ferroelectrics, *Science*, 2018, **361**, 151–155.

14 M. Liao, Y. Liu, P. Cui, N. Qu, F. Zhou, D. Yang, T. Han, Z. Lai and J. Zhu, Modeling of alloying effect on elastic properties in BCC Nb-Ti-V-Zr solid solution: From unary to quaternary, *Comput. Mater. Sci.*, 2020, **172**, 109289.

15 A. Marmier, Z. A. D. Lethbridge, R. I. Walton, C. W. Smith, S. C. Parker and K. E. Evans, ElAM: A computer program for the analysis and representation of anisotropic elastic properties, *Comput. Phys. Commun.*, 2010, **181**, 2102–2115.

16 M. de Jong, W. Chen, H. Geerlings, M. Asta and K. A. Persson, A database to enable discovery and design of piezoelectric materials, *Sci. Data*, 2015, **2**, 150053.

17 P. Ravindran, L. Fast, P. A. Korzhavyi, B. Johansson, J. Wills and O. Eriksson, Density functional theory for calculation of elastic properties of orthorhombic crystals: Application to $TiSi_2$, *J. Appl. Phys.*, 1998, **84**, 4891–4904.

18 I. Azuri, E. Meirzadeh, D. Ehre, S. R. Cohen, A. M. Rappe, M. Lahav, I. Lubomirsky and L. Kronik, Unusually large Young's moduli of amino acid molecular crystals, *Angew. Chem., Int. Ed.*, 2015, **54**, 13566–13570.

19 R. Feng, J.-H. Fan, K. Li, Z.-G. Li, Y. Qin, Z.-Y. Li, W. Li and X.-H. Bu, Temperature-responsive photoluminescence and elastic properties of 1D lead halide perovskites *R*- and *S*-(Methylbenzylamine)$PbBr_3$, *Molecules*, 2022, **27**, 728.

20 H. Wang, H. Liu, Z. Zhang, Z. Liu, Z. Lv, T. Li, W. Ju, H. Li, X. Cai and H. Han, Large piezoelectric response in a family of metal-free perovskite ferroelectric compounds from first-principles calculations, *npj Comput. Mater.*, 2019, **5**, 17.

21 K. Nakamura, S. Higuchi and T. Ohnuma, Density functional perturbation theory to predict piezoelectric properties, *Perturbation Methods with Applications in Science and Engineering*, 2018, pp. 2–7, DOI: 10.5772/intechopen.76827.

22 R. Pandey, G. Sb, S. Grover, S. K. Singh, A. Kadam, S. Ogale, U. V. Waghmare, V. R. Rao and D. Kabra, Microscopic Origin of piezoelectricity in lead-free halide perovskite: Application in nanogenerator design, *ACS Energy Lett.*, 2019, **4**, 1004–1011.

23 Y. Qin, F. F. Gao, S. Qian, T. M. Guo, Y. J. Gong, Z. G. Li, G. D. Su, Y. Gao, W. Li, C. Jiang, P. Lu and X. H. Bu, Multifunctional chiral 2D lead halide perovskites with circularly polarized photoluminescence and piezoelectric energy harvesting properties, *ACS Nano*, 2022, **16**, 3221–3230.

24 T.-M. Guo, F.-F. Gao, Z.-G. Li, Y. Liu, M.-H. Yu and W. Li, Mechanical and acoustic properties of a hybrid organic–inorganic perovskite, TMCM-$CdCl_3$, with large piezoelectricity, *APL Mater.*, 2020, **8**, 101106.

25 L. C. An, K. Li, Z. G. Li, S. Zhu, Q. Li, Z. Z. Zhang, L. J. Ji, W. Li and X. H. Bu, Engineering elastic properties of isostructural molecular perovskite ferroelectrics via B-site substitution, *Small*, 2021, **17**, 2006021.

26 T. M. Guo, Y. J. Gong, Z. G. Li, Y. M. Liu, W. Li, Z. Y. Li and X. H. Bu, A new hybrid lead-free metal halide piezoelectric for energy harvesting and human motion sensing, *Small*, 2022, **18**, 2103829.

27 K. Li, L.-Y. Dong, H.-X. Xu, Y. Qin, Z.-G. Li, M. Azeem, W. Li and X.-H. Bu, Electronic structures and elastic properties of a family of metal-free perovskites, *Mater. Chem. Front.*, 2019, **3**, 1678–1685.

28 S. Ippili, V. Jella, S. Eom, S. Hong and S. G. Yoon, Light-driven piezo- and triboelectricity in organic-inorganic metal trihalide perovskite toward mechanical energy harvesting and self-powered sensor application, *ACS Appl. Mater. Interfaces*, 2020, **12**, 50472–50483.

29 S. Ippili, V. Jella, J. Kim, S. Hong and S. G. Yoon, Unveiling predominant air-stable organotin bromide perovskite toward mechanical energy harvesting, *ACS Appl. Mater. Interfaces*, 2020, **12**, 16469–16480.

30 A. Sultana, P. Sadhukhan, M. M. Alam, S. Das, T. R. Middya and D. Mandal, Organo-lead halide perovskite induced electroactive beta-phase in porous PVDF films: An excellent material for photoactive piezoelectric energy harvester and photodetector, *ACS Appl. Mater. Interfaces*, 2018, **10**, 4121–4130.

31 G. Huang, A. A. Khan, M. M. Rana, C. Xu, S. Xu, R. Saritas, S. Zhang, E. Abdel-Rahmand, P. Turban, S. Ababou-Girard, C. Wang and D. Ban, Achieving ultrahigh piezoelectricity in organic–inorganic vacancy-ordered halide double perovskites for mechanical energy harvesting, *ACS Energy Lett.*, 2020, **6**, 16–23.

32 J. Lu, S. Hu, W. Li, X. Wang, X. Mo, X. Gong, H. Liu, W. Luo, W. Dong, C. Sima, Y. Wang, G. Yang, J. T. Luo, S. Jiang, Z. Shi and G. Zhang, A biodegradable and recyclable piezoelectric sensor based on a molecular ferroelectric embedded in a bacterial cellulose hydrogel, *ACS Nano*, 2022, **16**, 3744–3755.

33 W. Li, C. Li, G. Zhang, L. Li, K. Huang, X. Gong, C. Zhang, A. Zheng, Y. Tang, Z. Wang, Q. Tong, W. Dong, S. Jiang, S. Zhang and Q. Wang, Molecular ferroelectric-based flexible sensors exhibiting supersensitivity and multimodal capability for detection, *Adv. Mater.*, 2021, **33**, 2104107.

34 H. S. Wu, B. T. Murti, J. Singh, P. K. Yang and M. L. Tsai, Prospects of metal-free perovskites for piezoelectric applications, *Adv. Sci.*, 2022, **9**, 2104703.

35 H. S. Wu, S. M. Wei, S. W. Chen, H. C. Pan, W. P. Pan, S. M. Huang, M. L. Tsai and P. K. Yang, Metal-free perovskite piezoelectric nanogenerators for human-machine interfaces and self-powered electrical stimulation applications, *Adv. Sci.*, 2022, **9**, 2105974.

36 T. Vijayakanth, A. K. Srivastava, F. Ram, P. Kulkarni, K. Shanmuganathan, B. Praveenkumar and R. Boomishankar, A flexible composite mechanical energy harvester from a ferroelectric organoamino phosphonium salt, *Angew. Chem., Int. Ed.*, 2018, **57**, 9054–9058.

37 R. Ding, X. Zhang, G. Chen, H. Wang, R. Kishor, J. Xiao, F. Gao, K. Zeng, X. Chen, X. W. Sun and Y. Zheng, High-performance piezoelectric nanogenerators composed of formamidinium lead halide perovskite nanoparticles and poly(vinylidene fluoride), *Nano Energy*, 2017, **37**, 126–135.

38 W. Tong, Z. Wang, X. Wang, X. Zhang, Y. Zhang and Q. An, Self-powered materials obtained by interfacing functional assemblies with energy harvesting films, *Mater. Chem. Front.*, 2021, **5**, 2623–2648.

39 W.-Q. Liao, D. Zhao, Y.-Y. Tang, Y. Zhang, P.-F. Li, P.-P. Shi, X.-G. Chen, Y.-M. You and R.-G. Xiong, A molecular perovskite solid solution with piezoelectricity stronger than lead zirconate titanate, *Science*, 2019, **363**, 1206–1210.

40 Y. M. You, W. Q. Liao, D. Zhao, H. Y. Ye, Y. Zhang, Q. Zhou, X. Niu, J. Wang, P. F. Li, D. W. Fu, Z. Wang, S. Gao, K. Yang, J. M. Liu, J. Li, Y. Yan and R. G. Xiong, An organic-inorganic perovskite ferroelectric with large piezoelectric response, *Science*, 2017, **357**, 306–309.

41 J. Harada, T. Shimojo, H. Oyamaguchi, H. Hasegawa, Y. Takahashi, K. Satomi, Y. Suzuki, J. Kawamata and T. Inabe, Directionally tunable and mechanically deformable ferroelectric crystals from rotating polar globular ionic molecules, *Nat. Chem.*, 2016, **8**, 946–952.

42 H. P. Lv, W. Q. Liao, Y. M. You and R. G. Xiong, Inch-size molecular ferroelectric crystal with a large electromechanical coupling factor on par with barium titanate, *J. Am. Chem. Soc.*, 2022, **144**, 22325–22331.

43 Q. Pan, Y. A. Xiong, T. T. Sha and Y. M. You, Recent progress in the piezoelectricity of molecular ferroelectrics, *Mater. Chem. Front.*, 2020, **5**, 44–59.

44 D. W. Fu, J. X. Gao, W. H. He, X. Q. Huang, Y. H. Liu and Y. Ai, High-*Tc* enantiomeric ferroelectrics based on homochiral Dabco-derivatives (Dabco = 1,4-Diazabicyclo[2.2.2]octane), *Angew. Chem., Int. Ed.*, 2020, **59**, 17477–17481.

45 Y. Zhang, Y. Liu, H. Y. Ye, D. W. Fu, W. Gao, H. Ma, Z. Liu, Y. Liu, W. Zhang, J. Li, G. L. Yuan and R. G. Xiong, A molecular ferroelectric thin film of imidazolium perchlorate that shows superior electromechanical coupling, *Angew. Chem., Int. Ed.*, 2014, **53**, 5064–5068.

46 H. S. Choi, S. Li, I. H. Park, W. H. Liew, Z. Zhu, K. C. Kwon, L. Wang, I. H. Oh, S. Zheng, C. Su, Q. H. Xu, K. Yao, F. Pan and K. P. Loh, Tailoring the coercive field in ferroelectric metal-free perovskites by hydrogen bonding, *Nat. Commun.*, 2022, **13**, 794.

47 Y. Hu, Z. Liu, C. C. Wu, J. L. Gottfried, R. Pesce-Rodriguez, S. D. Walck, P. W. Chung and S. Ren, Chemically driven

energetic molecular ferroelectrics, *Nat. Commun.*, 2021, **12**, 5696.

48 Y. Li, Y. Du, C. R. Huang, H. Peng, Y. L. Zeng, J. C. Liu and W. Q. Liao, Homochiral anionic modification toward the chemical design of organic enantiomeric ferroelectrics, *Chem. Commun.*, 2021, **57**, 5171–5174.

49 Y. Shang, R.-K. Huang, S.-L. Chen, C.-T. He, Z.-H. Yu, Z.-M. Ye, W.-X. Zhang and X.-M. Chen, Metal-free molecular perovskite high-energetic materials, *Cryst. Growth Des.*, 2020, **20**, 1891–1897.

50 W.-J. Xu, Y. Zeng, W. Yuan, R.-G. Qiu, W.-X. Zhang and X.-M. Chen, Room-temperature optic-electric duple bistabilities induced by plastic transition, *Chem. Commun.*, 2018, **54**, 3347–3350.

51 Z.-Y. Li, X. Cao, X.-X. Li, Q. Jia and S.-Q. Zhang, Synthesis, characterization and hygroscopicity testing of molecular perovskite energetic materials, *Chin. J. Energ. Mater.*, 2020, **28**, 539–543.

52 X.-X. Chen, X.-Y. Zhang, D.-X. Liu, R.-K. Huang, S.-S. Wang, L.-Q. Xiong, W.-X. Zhang and X.-M. Chen, Room-temperature ferroelectric and ferroelastic orders coexisting in a new tetrafluoroborate-based perovskite, *Chem. Sci.*, 2021, **12**, 8713–8721.

53 K. Aizu, Possible species of ''Ferroelastic'' crystals and of simultaneously ferroelectric and ferroelastic crystals, *J. Phys. Soc. Jpn.*, 1969, **27**, 387–396.

54 K. Wagner, P. Cheng and D. Vezenov, Noncontact method for calibration of lateral forces in scanning force microscopy, *Langmuir*, 2011, **27**, 4635–4644.

55 S.-L. Chen, Z.-R. Yang, B.-J. Wang, Y. Shang, L.-Y. Sun, C.-T. He, H.-L. Zhou, W.-X. Zhang and X.-M. Chen, Molecular perovskite high-energetic materials, *Sci. China Mater.*, 2018, **61**, 1123–1128.

56 Y. Shang, Z.-H. Yu, R.-K. Huang, S.-L. Chen, D.-X. Liu, X.-X. Chen, W.-X. Zhang and X.-M. Chen, Metal-free hexagonal perovskite high-energetic materials with NH_3OH^+/$NH_2NH_3^+$ as B-site cations, *Engineering*, 2020, **6**, 1013–1018.

57 J. I. Pankove and H. Schade, Photoemission from GaN, *Appl. Phys. Lett.*, 1974, **25**, 53–55.

58 C. J. H. Wort and R. S. Balmer, Diamond as an electronic material, *Mater. Today*, 2008, **11**, 22–28.

59 W. Q. Liao, Y. Zhang, C. L. Hu, J. G. Mao, H. Y. Ye, P. F. Li, S. D. Huang and R. G. Xiong, A lead-halide perovskite molecular ferroelectric semiconductor, *Nat. Commun.*, 2015, **6**, 7338.

60 Y. Y. Chen, C. H. Gao, T. Yang, W. J. Li, H. J. Xu and Z. H. Sun, Research advances of ferroelectric semiconductors of 2D hybrid perovskites toward photoelectronic applications, *Chin. J. Struct. Chem.*, 2022, **41**, 2204001.

61 H. Park, C. Ha and J.-H. Lee, Advances in piezoelectric halide perovskites for energy harvesting applications, *J. Mater. Chem. A*, 2020, **8**, 24353–24367.

62 T. Vijayakanth, S. Sahoo, P. Kothavade, V. Bhan Sharma, D. Kabra, J. K. Zareba, K. Shanmuganathan and R. Boomishankar, A ferroelectric aminophosphonium cyanoferrate with a large electrostrictive coefficient as a piezoelectric nanogenerator, *Angew. Chem., Int. Ed.*, 2023, **135**, e202214984.

63 R. Gupta, S. Sahoo, S. Deswal, P. Kothavade, P. Dixit, J. K. Zareba, K. Shanmuganathan and R. Boomishankar, A flexible energy harvester from an organic ferroelectric ammonium salt, *Chem. – Asian J.*, 2021, **16**, 4122–4129.